Int. J. Heat Mass Transfer. Vol. 17, pp. 439–451. Pergamon Press 1974. Printed in Great Britain

LAMINAR BURNING BETWEEN PARALLEL FUEL SURFACES

J. S. KIM and J. DE RIS

Factory Mutual Research Corporation, 1151 Boston-Providence Turnpike, Norwood, Mass. 02062, U.S.A.

and

F. WILLIAM KROESSER
Tufts University, Medford, Mass., U.S.A.

(*Received* 16 *May* 1973 *and in revised form* 7 *September* 1973)

Abstract—A theoretical and experimental study is made of the factors influencing the burning rate between two vertical parallel fuel surfaces facing one another. No radiation, infinite gas phase reaction rates and unit Lewis number are assumed.

The equations are solved numerically and the burning rate is found to be controlled by the product of Grashof number and channel aspect ratio (i.e. the half channel width divided by its length). For a wide channel separation, the burning rate is independent of the channel separation distance and the results reduce to our previous solution for single surface burning. For very long narrow channels the burning rate becomes independent of the channel length and asymptotically approaches an analytical solution for infinitely long channels.

Finally, the theoretical results are compared to the experimental data with favorable agreement.

NOMENCLATURE

B, mass transfer driving force, see equation (18);
b, half channel separation distance [L];
C_p, specific heat [E/Mθ];
D, gas diffusivity [L^2/t];
F, normalized energy-specie function, see equation (25);
G, density function, see equation (32);
Gr, Grashof number $(gb^3/\nu_w^2)(L/C_pT_\infty)$;
g, gravitational force [L/t^2];
H, dimensionless channel height, see equation (45);
h, specific enthalpy relative to ambient temperature [E/M];
k, thermal conductivity [E/Ltθ];
L, effective heat of vaporization [E/M];
Le, Lewis number, $k/\rho C_pD$;
l, channel height [L];
M, molecular weight [M/mole];
$\dot{m}''$, mass flux at surface [M/L^{2}t];
$\dot{m}'''$, volumetric mass generation rate [M/L^{3}t];
Pr, Prandtl number, $C_p\mu/k$;
p, pressure [M/Lt^2];
p_0, ambient static pressure [M/Lt^2];
Q, heat of combustion (lower) for ν_F' moles of fuel [E];
$\dot{q}'''$, volumetric heat generation [E/L^{3}t];
R, universal gas constant [E/mole θ];
r, stoichiometric mass ratio of fuel to oxidant, see equation (30);
T, absolute temperature [θ];
U, dimensionless longitudinal velocity, see equation (44);
u, longitudinal velocity [L/t];
u_m, local maximum longitudinal velocity [L/t];
v, transverse velocity [L/t];
X, dimensionless longitudinal coordinate, see equation (21);
x, longitudinal coordinate [L];
Y, mass fraction;
Y, normalized transverse coordinate y/b in Appendix;
y, transverse coordinate [L];
Z, normalized dimensionless transverse coordinate, see equation (22);
Z_b, dimensionless half channel separation distance, see equation (22).

Greek symbols

α, generalized molecular diffusivity [L^2/t] in Appendix;
β_1, β_2, energy-specie functions, see equations (8) and (9);
γ, dimensionless ambient temperature, $\bar{C}_pT_\infty/L$;

Γ, generalized transferred property in Appendix;
μ, dynamic viscosity [M/Lt];
ν, kinematic viscosity [L^2/t];
ν', ν'', stoichiometric coefficients for reactants and products;
π, dimensionless excess pressure, see equation (24);
ρ, density [M/L^3];
τ, dimensionless surface temperature, $\frac{1}{2}\int_{T_s}^{T_{\infty}} C_p \mathrm{d}T$;
ψ, dimensionless stream function, see equation (23).

Subscripts
F, fuel;
f, flame;
in, entrance;
O, oxidant;
s, surface;
vap, vaporization;
w, fuel surface;
∞, ambient.

1. INTRODUCTION

THIS is a theoretical and experimental study of the factors influencing the laminar burning rates of two vertical parallel fuel surfaces facing one another. The study is motivated by the possibility of developing a standard materials flammability test wherein a subject material burns entirely within its own radiative and combustion environment. The study itself is designed to gain a deeper scientific insight into the physical factors controlling the burning rate. In addition, the channel burning problem in itself is of considerable practical importance.

It has frequently been observed that the free convective burning between two solid-fuel surfaces is considerably more intense than the burning of a single surface in the open. For example a single thick plank of wood does not burn in the open; however, two parallel planks, when placed a few centimeters apart, burn vigorously. This phenomenon has usually been attributed to three possible causes: (1) the containment of radiation being emitted by flames or hot solid surfaces inside the channel; (2) the so-called fluid dynamic "chimney effect" involving the confinement of hot combustion products; and (3) the prevention of possible gas-phase chemical kinetic extinction phenomena by increasing the gas flow times. While all three explanations have been proposed in the past, it is clear from the present study that only the first and third explanations are relevant since the fluid dynamic confinement actually causes a decrease in steady burning rate by restricting the access of oxidant to the fire.

This analysis ignores radiative effects. Since the fuel surfaces face one another, essentially all the radiant output from each surface is received by the opposite surface, thereby minimizing this effect. The flame radiation may be important, especially for those fuels with high flame temperature. Since the radiant output reduces both the flame temperature and the convective heat transfer, it is anticipated that its effect is partly self-cancelling for the confined flames considered here. In view of the present ignorance of flame radiation laws, this hypothesis should be checked experimentally.

The present problem is solved using Schvab-Zeldovich [1] variables ignoring gas-phase kinetics. Such a treatment of diffusive burning phenomena is conventional and burning problems of different geometries have been solved in this manner by Spalding [2], Emmons [3], de Ris [4], Kosdon, Williams and Buman [5], and Kim, de Ris and Kroesser [6]. The related free convective heat transfer problems for the parallel geometry used in this study were also considered by Elenbaas [7], Boida and Osterle [8], Worsøe-Schmidt and Leppert [9], Lawrence and Chato [10], Davis and Perona [11], Quintiere and Mueller [12] and many others.

2. GOVERNING EQUATIONS

The schematic diagram of the vertical parallel fuel-beds which are transferring fuel by convection and diffusion into the gas-phase is shown in Fig. 1. The

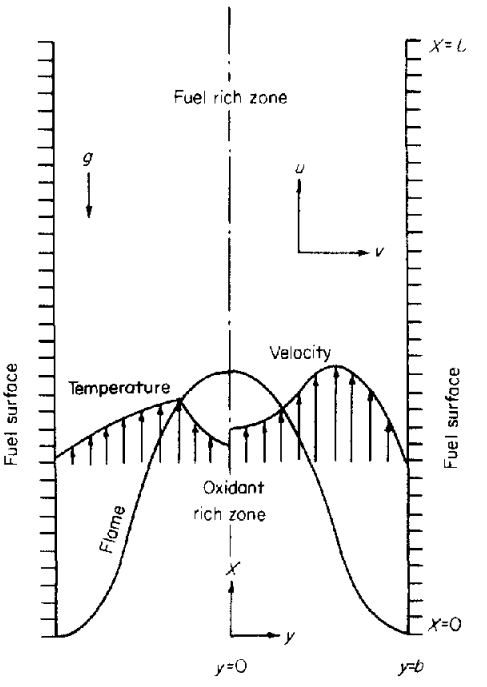

FIG. 1. Schematic diagram of the problem.

oxidant is introduced at the bottom entrance by the natural convection induced by the hot reaction gases. If the channel is sufficiently narrow and high, the oxidant is entirely consumed in the region below the flame inside the channel, thereby preventing its existence above the flame. In this case, the channel is clearly divided into two zones, an oxidant-rich zone below and a fuel-rich zone above the flame. The present theory solves the steady state laminar burning of the above geometry.

Here x and y are, respectively, the longitudinal and transverse coordinates, while u and v are the corresponding velocity components. The gravitational force is acting vertically downward and the channel has a length, l, and a half separation distance, b. The equations for a steady state laminar diffusion flame within a free convective boundary layer are as follows:

Conservation of Mass:

$$\frac{\partial}{\partial x}(\rho u)+\frac{\partial}{\partial y}(\rho v)=0 \tag{1}$$

Conservation of Momentum:

$$u\frac{\partial u}{\partial x}+v\frac{\partial u}{\partial y}=-\frac{1}{\rho}\frac{\partial p}{\partial x}-g+\frac{1}{\rho}\frac{\partial}{\partial y}\left(\mu\frac{\partial u}{\partial y}\right) \tag{2}$$

Conservation of Energy:

$$u\frac{\partial h}{\partial x}+v\frac{\partial h}{\partial y}=\frac{1}{\rho}\frac{\partial}{\partial y}\left(\frac{k}{C_p}\frac{\partial h}{\partial y}\right)+\dot{q}''' \tag{3}$$

where

$$h\equiv\int_{T_\infty}^{T}C_p\mathrm{d}T$$

is the specific enthalpy.

Conservation of Specie, "i",:

$$u\frac{\partial Y_i}{\partial x}+v\frac{\partial Y_i}{\partial y}=\frac{1}{\rho}\frac{\partial}{\partial y}\left(\rho D\frac{\partial Y_i}{\partial y}\right)+\dot{m}_i''' \tag{4}$$

State:

$$\rho T=\rho_\infty T_\infty. \tag{5}$$

Here $\dot{q}'''$ and $\dot{m}_i'''$ are, respectively, the volumetric heat and mass "i" generation rates. These equations presume ideal gases, no thermally driven specie diffusion, and no radiation. The transport properties, μ, k/C_p, and ρD are assumed to be independent of composition with unit Lewis number $Le=\rho C_pD/k$. Also, the longitudinal diffusive transfer of heat, momentum and species is ignored. This latter approximation is examined in the Appendix. Equation (5) is obtained by assuming velocities much less than the speed of sound and all species having equal molecular weights. The specific heat, C_p is assumed to be identical for all species but can depend on temperature.

The source terms $\dot{q}'''$ and $\dot{m}_i'''$ are related by the overall stoichiometric equation (which assumes infinite gas-phase reaction rates):

$$\nu_F' \text{ Fuel}+\nu_0' \text{ Oxidant}\rightarrow\nu_p'' \text{ Product}+Q \text{ Heat} \tag{6}$$

where Q is the heat released by the combustion of $M_0\nu_0'$ or $M_F\nu_F'$ mass of oxidant or fuel respectively. Thus, within the flame zone,

$$\frac{\dot{m}_F'''}{M_F\nu_F'}=\frac{\dot{m}_0'''}{M_0\nu_0'}=-\frac{\dot{q}'''}{Q}. \tag{7}$$

Similar relations can be established between heat and any particular specie or between species; however, the fuel, oxidant and heat are of primary interest in the present problem.

By defining two Schvab–Zeldovich [1] variables which are conserved throughout in the gas phase.

$$\beta_1\equiv[h+(Y_0-Y_{0\infty})Q/M_0\nu_0']/L \tag{8}$$

$$\beta_2\equiv[h+Y_FQ/M_F\nu_F']/L. \tag{9}$$

Equations (3) and (4) are reduced with equation (7) to the homogeneous equations:

$$u\frac{\partial\beta_i}{\partial x}+v\frac{\partial\beta_i}{\partial y}-\frac{1}{\rho}\frac{\partial}{\partial y}\left(\frac{k}{C_p}\frac{\partial\beta_i}{\partial y}\right)=0,\ i=1,2. \tag{10}$$

Here, equation (10) is obtained by assuming the heat transfer occurs in the same manner as specie transfer, i.e. the Lewis number, $\rho C_pD/k=1$. The "effective heat of vaporization", L, is the ratio of total heat transfer to the surface to the total outgoing mass from the surface which for steady burning of a fuel supplied from a reservoir at T_∞ is

$$L=\frac{\dot{q}''}{\dot{m}_F''}=L_{T_{vap}}+\int_{T_\infty}^{T_{vap}}C_{p_i}\mathrm{d}T$$

where T_{vap} and C_{p_i} are, respectively, the temperature at which the fuel vaporizes and the condensed fuel specific heat. The effective heat of vaporization is presumed to be constant throughout this problem which enables T_{vap} also to be a constant. For completely steady burning with fuel being supplied from a constant temperature reservoir at T_∞ the energy conducted into the fuel interior is exactly equal to the energy transfer required to heat the fuel to its vaporization temperature prior to vaporization. Under such steady conditions and in the absence of radiation we previously showed [6] quite generally that T_{vap} is constant for unit Lewis number, rapid gas phase kinetics and quasi-equilibrium vaporization such as occurs for a liquid or subliming solid fuel. If there is no heat loss to the fuel bed interior and the gas and condensed phases are in equilibrium at the surface, then the above defined L is identical to the conventional heat of vaporization or sublimation of the fuel, $L_{T_{vap}}$ evaluated at the surface temperature.

3. BOUNDARY CONDITIONS

At the entrance, it is clear by the definitions of β_1 and β_2,

$$\text{at } x = 0, \beta_1 - \beta_2 = 0. \tag{11}$$

The velocity at the entrance can be obtained by integrating the Bernoulli equation for a horizontal stream line considering the entrance as a mass sink. Thus,

$$\text{at } x = 0, p - p_0 = -(\rho_\infty u_{\text{in}}^2)/2 \tag{12}$$

where p_0 is the ambient static pressure at level $x = 0$ and u_{in} is the inlet velocity at the entrance which is uniform across the channel at this level. This u_{in} will be used as an "eigenvalue" for the problem since it is also determined by the combustion taking place in the channel.

At the exit, the pressure equals the ambient pressure at the exit height, since flow separation occurs at the exit; thus,

$$\text{at } x = l, p = p_0 - \rho_\infty g l. \tag{13}$$

At the center line of the channel, the geometrical symmetry gives

$$\text{at } y = 0$$

$$\frac{\partial u}{\partial y} = 0 \tag{14}$$

$$\frac{\partial \beta_i}{\partial y} = 0, \; i = 1, 2. \tag{15}$$

At the fuel surface, the longitudinal velocity is zero assuming no slipping flow and the mass flux at the surface is proportional to the heat flux to the surface; thus,

$$\text{at } y = b$$

$$u = 0 \tag{16}$$

$$\dot{m}_F'' = \rho v = \frac{1}{L}\frac{k}{C_p}\frac{\partial h}{\partial y}. \tag{17}$$

We now consider the boundary conditions for the energy-specie equations at the surface. In this problem, the fuel surface is regarded to be at its vaporization temperature, T_{vap}, which for steady burning lies a few degrees below the boiling temperature. For methanol as fuel, this temperature was calculated to be 328°K [13] (normal boiling point 337·7°K) using the Antoin equation [14] coupled with this theory. Noting that for infinitely fast reactions no oxidant exists at the surface, one obtains from the definition of β_1,

$$\text{at } y = b, \beta_1 = -\left(\frac{Y_{0\infty}Q}{M_0 v_0'} - h_{\text{vap}}\right)\Big/ L \equiv -B \tag{18}$$

where

$$h_{\text{vap}} \equiv \int_{T_\infty}^{T_{\text{vap}}} C_p \mathrm{d}T.$$

Now, the value of β_2 at the surface is not immediately obvious since Y_F is unknown there. However, the fuel transferred into the gas phase is carried out by both convection and diffusion; thus at the surface,

$$y = b, \dot{m}_F'' = \rho v Y_F - \rho D \frac{\partial Y_F}{\partial y}, \tag{19}$$

and, using unit Lewis number and equation (17), one obtains the relationship of the gradients of the two defined energy-specie functions:

$$\text{at } y = b,$$

$$\frac{\partial \beta_2}{\partial y} = \left(1 - \frac{Q}{M_F v_F' L} + \beta_2(x, b) - \frac{h_{\text{vap}}}{L}\right)\frac{\partial \beta_1}{\partial y}. \tag{20}$$

4. TRANSFORMATION OF EQUATIONS TO THEIR DIMENSIONLESS FORMS

The equations and boundary conditions will now be transformed into their dimensionless forms. The independent dimensionless variables are defined as

$$X \equiv \frac{v_w^2}{g}\left(\frac{C_p T_\infty}{L}\right)\left(\frac{\rho_w}{\rho_\infty}\right)^4 \frac{x}{b^4} \tag{21}$$

$$Z \equiv \frac{1}{Z_b}\int_0^{y/b} \frac{\rho}{\rho_\infty} \mathrm{d}\left(\frac{y}{b}\right) \text{ where } Z_b(X) \equiv \int_0^1 \frac{\rho}{\rho_\infty} \mathrm{d}\left(\frac{y}{b}\right) \tag{22}$$

so that $Z = 0$ is at the centerline and $Z = 1$ is at the surface. The transverse coordinate Z is a Howarth [15] transformed normalized distance which eliminates the variable density, ρ, in the governing equations with the aid of a dimensionless stream function which automatically satisfies the conservation of mass equation (1), namely:

$$\psi \equiv \frac{v_w}{g b^2}\left(\frac{C_p T_\infty}{L}\right)\left(\frac{\rho_w}{\rho_\infty}\right)^2 \int_0^{y/b} \left(\frac{\rho}{\rho_\infty}\right) u \, \mathrm{d}\left(\frac{y}{b}\right) \tag{23}$$

which for convenience is also zero along the center line ($Z = 0$). The dimensionless excess pressure over that of the ambient gas at the same level is defined as

$$\pi \equiv \frac{v_w^2}{\rho_\infty g^2 b^4}\left(\frac{C_p T_\infty}{L}\right)^2 \left(\frac{\rho_w}{\rho_\infty}\right)^4 (p - p_0 + \rho_\infty g x). \tag{24}$$

The two energy-specie functions, β_1 and β_2 are proportional throughout the gas phase since they are governed by the identical governing equation, equations (10), and are proportional at the center line, fuel surface and entrance, equations (15), (20) and (11) respectively. This argument enables one to define a new normalized energy-specie function as

$$F(X, Z) \equiv -\frac{\beta_1(X, Z)}{B} = \frac{\beta_2(X, Z)}{\beta_2(X, 1)}. \tag{25}$$

Thus, F is unity at the fuel surface and zero for the pure oxidant at the entrance. Solving these equations

for equation (20), one obtains the surface relation,

$$\beta_2(X,1)=\frac{B}{B+1}\left(\frac{h_{vap}}{L}+\frac{Q}{M_F v'_F L}-1\right).$$

Using the above defined variables, one can transform the energy-specie equation, equation (10) to its new form,

$$Z_b\psi_Z F_X - Z_b\psi_X F_Z - \frac{1}{Pr}F_{ZZ}=0 \tag{26}$$

where $\rho\mu/Pr=\rho^2 D=\rho k/C_p$ are assumed to be constant with the unit Lewis number and the numerical value of $\rho\mu$ is calculated at the surface condition, $\rho_w\mu_w$.

To transform the momentum equation, one needs to express the variable density in terms of the local enthalpy; thus, assuming constant specific heat for this term, with equation (5) one has:

$$\frac{\rho_\infty-\rho}{\rho}=\frac{T-T_\infty}{T_\infty}=\frac{h}{\bar{C}_p T_\infty}$$

where $\bar{C}_p$ is chosen to provide the correct density ratio at the flame. Since there is no oxidant in the fuel rich zone and no fuel in the oxidant-rich zone, β_1 and β_2 can be used to express the above equation as

$$\frac{\rho_\infty-\rho}{\rho}=\frac{L}{\bar{C}_p T_\infty}\left(\beta_1+\frac{Y_{0\infty}Q}{M_0 v'_0 L}\right) \quad \text{in the fuel-rich zone}$$
$$=\frac{L}{\bar{C}_p T_\infty},\beta_2 \quad \text{in the oxidant-rich zone.} \tag{27}$$

These equations will now be expressed in terms of the normalized energy-specie function F defined above as well as the dimensionless parameters,

$$\gamma\equiv\frac{\bar{C}_p T_\infty}{L} \tag{28}$$

$$\tau\equiv\frac{h_{vap}}{L} \tag{29}$$

$$r\equiv Y_{0\infty}\frac{M_F v'_F}{M_0 v'_0}. \tag{30}$$

Physically γ, τ and r are respectively the dimensionless ambient temperature, the dimensionless fuel surface temperature and the stoichiometric mass ratio of fuel to oxidant. At the flame, the infinitely fast reactions do not permit fuel and oxidant to coexist, so that at the flame $\beta_2-\beta_1=Y_{0\infty}Q/M_0 v'_0 L$; and using the above parameters and F, one has

$$F_f=\frac{B+1}{B}\frac{r}{r+1} \text{ at the flame.} \tag{31}$$

Equation (27) can now be expressed as

$$(\rho_\infty-\rho)/\rho=G(F)/\gamma \tag{32}$$

where $G(F)=\tau+B\{1-F(X,Z)\}$

when $F\geqslant F_f$ (i.e. fuel-rich zone)

$$G(F)=\left(\frac{B+\tau}{F_f}-B\right)F(X,Z)$$

when $F\leqslant F_f$ (i.e. oxidant-rich zone)

with the above density functions being identical at the flame, i.e. $F=F_f$.

The governing momentum equation with its variable density term becomes

$$\psi_{ZZZ}+Z_b\psi_X\psi_{ZZ}-Z_b\psi_Z\psi_{XZ}+Z_{b_X}\psi_Z^2 - Z_b^3\left(\frac{G(F)}{\gamma}+1\right)\pi_X+Z_b^3 G(F)=0. \tag{33}$$

The dimensionless, half-separation distance, Z_b, defined previously by equation (22) becomes

$$Z_b(X)=\frac{1}{\int_0^1\left(\frac{G(F)}{\gamma}+1\right)dZ}.$$

Finally, the boundary conditions developed in the previous section are:

At the entrance, $X=0$,

$$F=0 \tag{34}$$

$$\psi_Z=U_{in} \tag{35}$$

$$\pi=-U_{in}^2/2. \tag{36}$$

At the center line, $Z=0$,

$$F_Z=0 \tag{37}$$

$$\psi_{ZZ}=0 \tag{38}$$

$$\psi=0. \tag{39}$$

At the fuel surface, $Z=1$,

$$\psi_Z=0 \tag{40}$$

$$F=1 \tag{41}$$

$$\psi_X=\frac{1}{Z_b}\frac{B}{Pr}F_Z. \tag{42}$$

And at the exit, $X=H$,

$$\pi=0 \tag{43}$$

where the dimensionless inlet velocity and the height of the channel are defined as

$$U_{in}\equiv\frac{v_w}{gb^2}\left(\frac{C_p T_\infty}{L}\right)\left(\frac{\rho_w}{\rho_\infty}\right)^2 u_{in} \tag{44}$$

$$H\equiv\frac{v_w^2}{g}\left(\frac{C_p T_\infty}{L}\right)\left(\frac{\rho_w}{\rho_\infty}\right)^4\frac{l}{b^4}. \tag{45}$$

5. THEORETICAL RESULTS

Using the theory developed in the previous sections, three typical fuels, *n*-heptane, methanol and α-cellulose were calculated for a wide range of channel heights and separations. The parameters for these fuels used in the calculations are given in Table 1.

Table 1. Dimensionless parameters for fuels

Parameter	Symbol	*n*-Heptane	Methanol	α-Cellulose*
Mass transfer driving force	B	8·56	2·5	1·0
Surface temperature	τ	0·26	0·04	0·16
Ambient temperature	γ	1·15	0·338	0·16
Stoichiometric mass ratio	r	0·066	0·155	0·14
Prandtl number	Pr	0·74	0·74	0·74

*Based on the experiments of Kosdon, Williams and Buman [5] and theoretical work of Kim, de Ris and Kroesser [6].

The governing parabolic equations are numerically solved with the Predictor-Corrector method [16] using backward differences in the X-direction. The initial velocity, U_{in} is presumed to be known across the entrance and its corresponding channel height, H, is calculated by marching in the X-direction until the exit condition, $\pi = 0$ [equation (43)] is reached. The numerical solution was always continued until we were absolutely sure that no further solutions were possible; that is, the gases must be cooled to the wall temperature, T_{vap}, of the fully saturated fuel vapor and the excess pressure must be diverging from $\pi = 0$.

Figures 2 and 3 show the pressure changes for burning methanol and α-cellulose inside the channel for different values of U_{in}. The normalized pressures start at minus unity at the entrance in accordance with the initial condition, equation (36). For methanol, there are three types of π vs X curves having zero, one or two values of H for which $\pi = 0$ corresponding respectively to zero, one or two solutions (i.e. heights, H). The methanol pressure curves intersecting $\pi = 0$ at large values of H indicate two points where the interior pressure in the channel equals the ambient pressure. Thus, the exit condition, $\pi = 0$, is necessary but not sufficient for an exit. The curves for very large values of U_{in} have a similar shape, but the greater initial pressure drop due to friction losses prevents the buoyancy from bringing these curves back to $\pi = 0$; this means that no physically realistic free convective solutions exist for such large values of U_{in}.

In terms of channel height, or more precisely $H \sim l/b^4$, the inlet velocity, U_{in}, increases with increasing channel height until U_{in} reaches a maximum (for methanol this is $4{\cdot}084 \times 10^{-3}$). With further increases in H, U_{in} decreases and asymptotically approaches a finite value (for methanol, $2{\cdot}76 \times 10^{-3}$) which for infinitely long channels corresponds to zero excess pressure gradient for downstream. Such behavior at large heights is characteristic of liquid fuels which have relatively low vaporization temperatures and large mass transfer rates resulting in the friction loss overcoming buoyancy with an eventual decrease in pressure.

Figure 3 on the other hand shows the excess pressure curves for α-cellulose, a solid-fuel. For actual burning of α-cellulose, the gaseous fuel is generated by pyrolysis —a non-equilibrium process with increasing char-deposition at the surface, preventing a truly steady state burning. Nevertheless it is worthwhile to investigate the mean burning phenomena of the pseudo-ideal α-cellulose representing effective physical data as interpreted in [5]. Only one or no solution occurs for each U_{in} as shown, since the excess pressure never does come back down to $\pi = 0$ after once exceeding $\pi = 0$. Within the channel, the excess pressure always remains less than zero. As H increase, U_{in} increases and asymptotically approaches $U_{in} = 3{\cdot}38 \times 10^{-3}$ which is the initial velocity for an infinitely long channel. Since α-cellulose has a small B number (implying a relatively low mass flux from the surface) and a high surface temperature, the problem is quite similar to the pure free convective heat transfer problem in a channel [11] which also shows only one zero for its pressure defect curve.

Figure 4 shows the dimensionless burning rate with respect to the dimensionless reciprocal height for three fuels over their whole range of channel heights and separations. Defining n as the slope of the log–log curves, the total burning rate becomes proportional to $l^{1-n}b^{4n-1}$. For the shorter or more widely separated channels on the right hand side of the figure, the curves have a quarter power slope (i.e. $n = 1/4$) with respect to reciprocal height, i.e. b^4/l. Thus, the total burning rate per unit channel length is proportional to $l^{3/4}b^0$; which is independent of the separation distance. Physically, this means that, in this open regime, a relatively

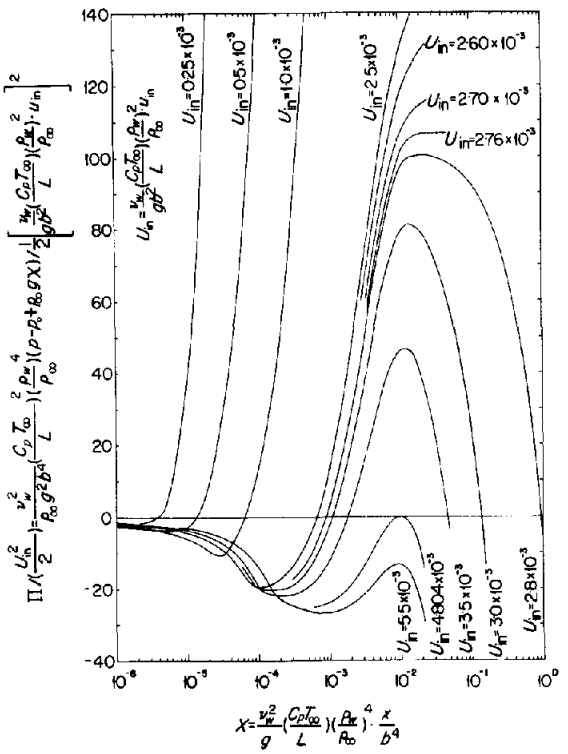

FIG. 2. Dimensionless normalized excess pressure curves within the channels for methanol.

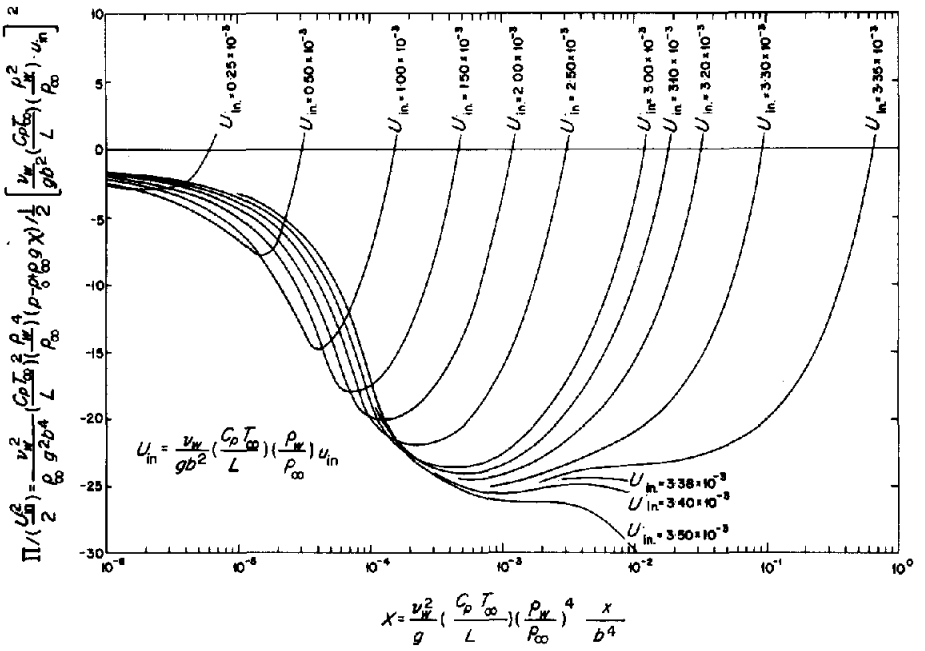

FIG. 3. Dimensionless normalized excess pressure curves within the channels for α-cellulose.

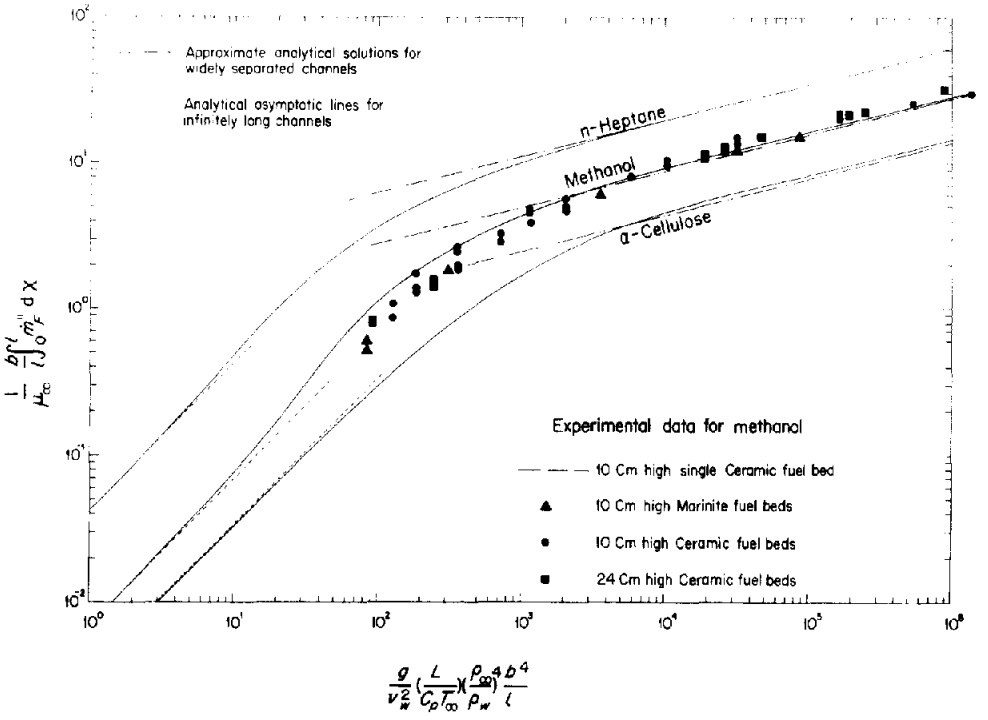

FIG. 4. Theoretical and experimental burning rates. Restricted regime on the left and open regime on the right.

large amount of oxidant is supplied and the burning becomes independent of the existence of the opposing surface. Thus, the solutions in this regime approach that of free convective burning of a single surface. Here, the burning rate asymptotically approaches our single-surface numerical solution [6] with a numerical discrepancy for methanol burning within 2 per cent. The asymptotic lines correspond to an analytical solution to be discussed in the next section.

As the height increases (i.e. b^4/l decreases) the supply of oxidant becomes restricted. If the channel is sufficiently high and narrow, the oxidant is entirely consumed near the entrance with the remaining height containing fuel-rich gases. In this restricted regime on the left hand side of Fig. 4, the slopes asymptotically approach unity (for the two liquid fuels from above and α-cellulose from below). In this regime the total burning rate per unit channel length is proportional to $l^0 b^3$; therefore, it becomes independent of the height of the channel, l, since the oxidant is totally consumed, after which the gases are cooled to the surface temperature.

Figures 5–7 show the stream lines, excess pressure changes, velocity, and temperature profiles for the burning of methanol in the open, intermediate and restricted regimes, respectively. All three channels are

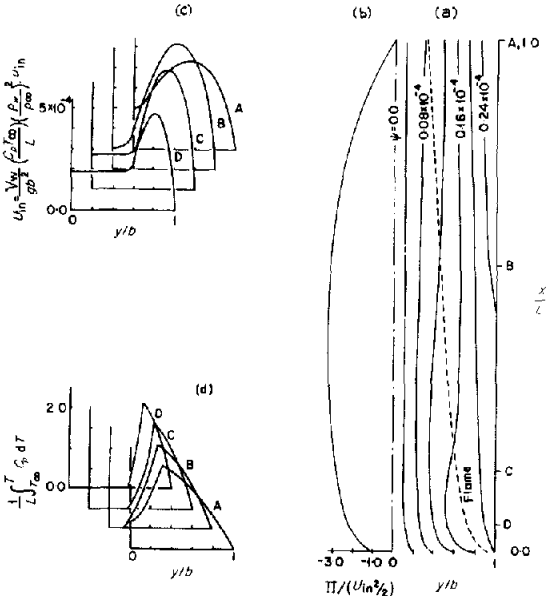

FIG. 5. Typical results in the open regime, methanol $H = 0{\cdot}3279 \times 10^{-5}$, $l/b = 5$ which implies $l = 8{\cdot}34$ cm $b = 1{\cdot}67$ cm for the particular value of H, (a) stream lines and flame shape; (b) dimensionless normalized excess pressure; (c) velocity at each level; (d) temperature at each level.

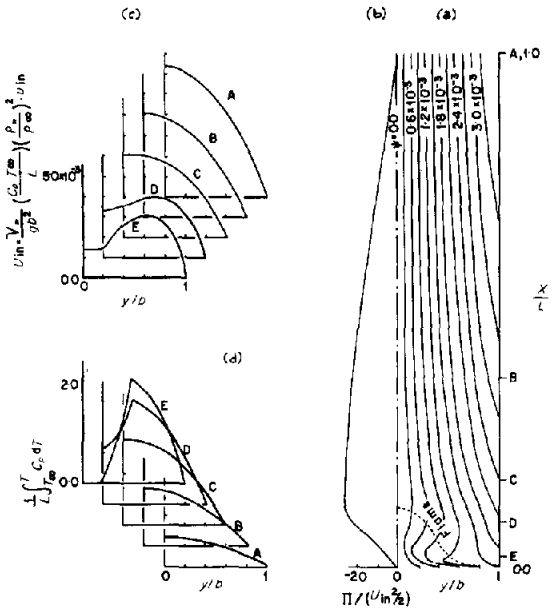

FIG. 6. Typical results in the intermediate regime, methanol, $H = 0{\cdot}36736 \times 10^{-4}$, $l/b = 5$ which implies $l = 3{\cdot}75$ cm, $b = 0{\cdot}75$ cm for the particular value of H, (a) stream lines and flame shape; (b) dimensionless normalized excess pressure; (c) velocity at each level; (d) temperature at each level.

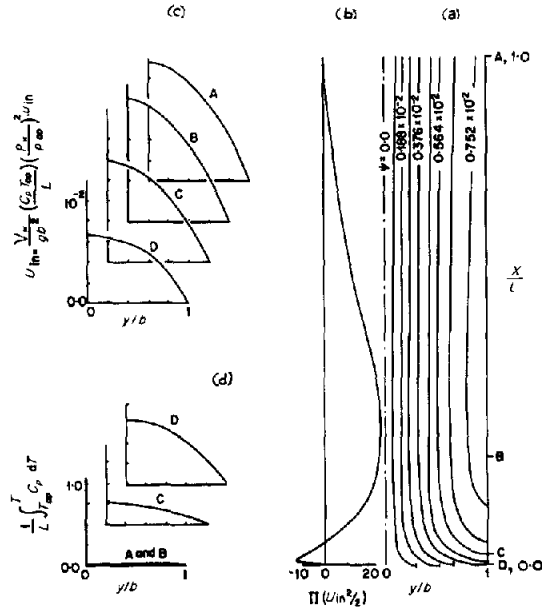

FIG. 7. Typical results in the restricted regime, methanol, $H = 0{\cdot}2578 \times 10^{-1}$, $l/b = 5$ which implies $l = 0{\cdot}42$ cm, $b = 0{\cdot}084$ cm for the particular value of H, (a) stream lines (flame shape is not shown because it occurs almost at the entrance); (b) dimensionless normalized excess pressure; (c) velocity at each level; (d) temperature at each level.

shown with a l/b ratio of 5. For this particular aspect ratio, the boundary layer approximation could introduce significant errors near the entrance as suggested by Figs. 6 and 7. However, for larger aspect ratios this type of error would be negligible as discussed in the Appendix.

The numerical error for these solutions is always maintained less than 3 per cent in terms of the resulting pressure distributions. This corresponds to a burning rate error of less than 1·5 per cent.

6. ASYMPTOTIC SOLUTIONS FOR THE OPEN AND RESTRICTED REGIMES AND THEIR INTERPRETATION

Approximate and exact analytical solutions are possible for open and very restricted regimes respectively, and these solutions are compared to the numerical results developed in the previous sections. Sometimes, these analytical solutions are more convenient and can be used to estimate burning rates for various applications.

For the widely separated regime, the burning rate approaches the single surface burning solution; thus, the approximate solution of the study [6] can be used directly. The burning rate derived from a Pohlhausen approximation procedure involving assumed velocity and energy-species profiles was shown to be

$$\dot{m}''_F = \left(\frac{9B\ln(1+B)}{40\,Pr}\right)^{1/2} \times \left\{\frac{\frac{3}{2}(B+\tau)(1-F_f^{2/3})+\tau}{\gamma(B+1)\left[Pr+\frac{5}{6}(B+1)\right]}\right\}^{1/4} (\rho_w^2\mu_w^2 g/x)^{1/4}. \quad (46)$$

Integrating this equation, we obtain

$$\frac{1}{\mu_\infty}\frac{b}{l}\int_0^l \dot{m}''_F\,dx = \left(\frac{B\ln(1+B)}{Pr}\right)^{1/2} \times \left\{\frac{6}{25}\frac{(B+\tau)(1-F_f^{2/3})+\tau}{(B+1)\left[Pr+\frac{5}{6}(B+1)\right]}\right\}^{1/4} \left(\frac{g}{\nu_w^2}\left(\frac{L}{C_pT_\infty}\right)\left(\frac{\rho_\infty}{\rho_w}\right)^4\frac{b^4}{l}\right)^{1/4}. \quad (47)$$

This approximate equation agrees to within 5 per cent of the exact burning rate in the open regime for all practical fuels.

In the restricted regime, an exact asymptotic solution can be obtained by considering an infinitely long channel. In such a channel, the velocity and temperature profiles become fully developed except for the relatively negligible portion near the entrance. The velocity profile is

$$u = u_m[1-(y/b)^2]. \quad (48)$$

Here, u_m is the maximum velocity which occurs at the center line $y = 0$. For such long channels both the inertia terms and the excess pressure gradient term are zero over essentially the entire length. Thus, the

momentum equation, equation (2), reduces to

$$g(\rho_\infty - \rho_w) - 2\mu_w \frac{u_m}{b^2} = 0 \quad (49)$$

where ρ_w is the density of gas in the channel.

Taking a mass and heat balance between entrance and exit, one has

$$\rho_w \int_0^b u \, dy = \tfrac{2}{3}\rho_w u_m b = \rho_\infty u_{in} b + \int_0^l \dot{m}''_F \, dx \quad (50)$$

$$\rho_\infty u_{in} b \frac{Y_{O\infty} Q}{M_O \nu'_O} = \rho_\infty u_{in} b C_p (T_{vap} - T_\infty) + L \int_0^l \dot{m}''_F \, dx. \quad (51)$$

Combining the above three equations with the definitions for B, τ, γ, one obtains the final burning rate equation for the restricted regime as

$$\frac{1}{\mu_\infty}\frac{b}{l}\int_0^l \dot{m}''_F \, dx = \frac{B}{3(B+1)} \tau \left(\frac{\gamma}{\tau+\gamma}\right)^3 \times \left(\frac{g}{\nu_w^2}\left(\frac{L}{C_p T_\infty}\right)\left(\frac{\rho_\infty}{\rho_w}\right)^4 \frac{b^4}{l}\right), \quad (52)$$

which has unity slope in the log–log plot of Fig. 4.

Next, the influence of the parameters on the total burning rate will be discussed. The burning rate is controlled by (1) the geometrical parameter, $Gr(b/l) \sim b^4/l$, whose effects were explained in the previous section; (2) mass transfer driving force, B, (3) surface temperature, τ, (4) stoichiometric fuel oxidant mass ratio, r, (5) ambient temperature, γ and (6) transport parameter Prandtl number, Pr. The Prandtl number is regarded as a constant and equal to that of air at ambient temperature. The effects of the parameters, B, τ and r in the open regime were described in detail by the authors in a previous study on single surface burning [6], with the conclusion that the burning rate is controlled primarily by the B number for common fuels.

The dimensionless ambient temperature parameter, $\gamma = \bar{C}_p T_\infty / L$ controls the thermal expansion of the gas with its consequent acceleration and flow blocking effects inside the channel. Thus, for small values of γ, the expansion is severe and the flow requires strong acceleration, thereby creating a blocking effect which discourages the influx of oxidant at the entrance and reduces the burning rate within the restricted regime associated with long and narrow channels. However, in the open regime the thermal expansion inside the channel is less important and the burning rate in this regime for the same H is independent of γ. The stoichiometric ratio, r, usually has only a minor effect on the burning rate in the open regime, and in the restricted regime the burning rate is totally independent of r.

The asymptotic solutions, equations (47) and (52), are plotted in Fig. 4 and compared to the numerical results of the three fuels.

7. EXPERIMENTS

Methanol was saturated in two identical porous slabs and burned in the vertical channel between facing slabs in ambient air as shown in Fig. 8. All surfaces except the facing surfaces were sealed with aluminum foil. The weight loss versus time was measured during flaming combustion and the results were compared with the theory.

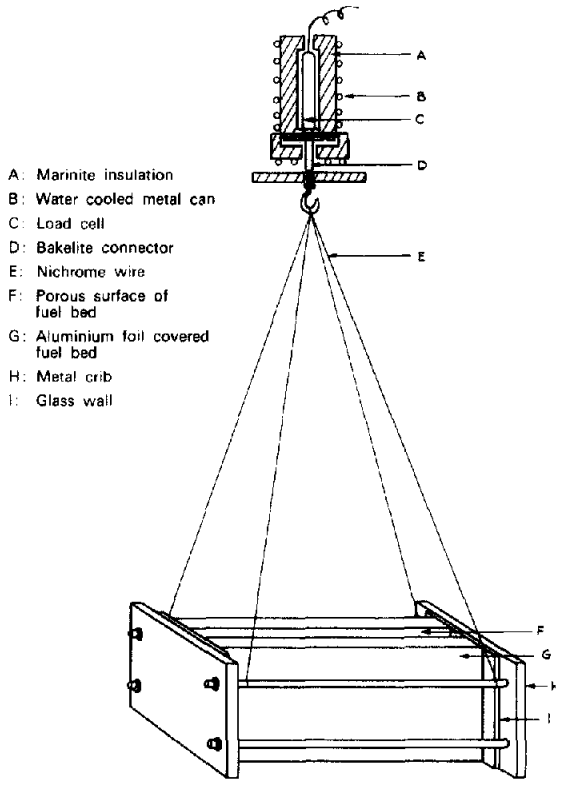

FIG. 8. Experimental arrangement.

The 10-cm and 24-cm high porous ceramic slabs (C-400 capillite formula made by Hamilton Porcelains Ltd) were used as fuel beds. Also, the effects of fuel bed porosity were checked by running tests with 10-cm high Marinite-23 (Johns Manville's somewhat less porous material) fuel beds with similar results.

The slabs were fixed in a metallic crib, separated by a specific distance, and lateral entrainment was prevented by glass end-walls. The crib was then secured by bolts and soaked for at least 5 min in a methanol tank to achieve thorough saturation. The unit was hung on a load cell to measure the weight loss versus

time during flaming combustion. The load cell was protected by a water-cooled metal can with Marinite insulation so that the weight loss rate measurements were affected by no more than 1 per cent due to the fire below. The weight loss curves showed steady burning after a very short initial transient period.

The results are shown in Fig. 4 with the theoretical calculations for methanol. In this data, the wall kinematic viscosity, ν_w, is calculated for the mixture of product gases and methanol vapor (mass fraction, 0·694 [13]) at the surface temperature, 328°K. Ambient gas viscosity was also calculated for the same mixture gas using the relation, $\mu_\infty = \mu_w(\rho_w/\rho_\infty)$ at the ambient temperature, 293°K.

The possible radiation heat loss was also tested by repeating the experiment with one of the slabs removed with results shown by the dash–dot line in Fig. 4. The theory predicts the same results for the single surface and the widely separated channels; thus, this discrepancy of the two experimental results, which are 10–15 per cent in burning rate, are interpreted as purely due to the radiation heat containment.

The theoretical results agree favorably with the experimental data over the entire range. For the open regime, the data clearly show a quarter-power relation with respect to b^4/l. As the separation distance decreases, or the height of the channel increases, the data show a moderate scatter which could be attributable to errors in measuring the very narrow gaps of the channel in this regime.

8. CONCLUSIONS

A given fuel shows three burning regimes depending on channel geometric arrangement, l/b^4. For shorter or more widely separated channels of small l/b^4, the burning is less dependent on the existence of the opposing surface and the total burning rate is proportional to the three-quarter power of height of channel. If the channel is sufficiently high and narrow, the oxidant is entirely consumed near the entrance and the total burning rate is independent of the channel height but proportional to the cube of the separation. Between the open and restricted regimes, there exists an intermediate regime.

The mass transfer driving force, B, is the dominant chemical parameter, whereas the dimensionless surface temperature, τ, the stoichiometric fuel-oxidant mass ratio, r, and the dimensionless ambient temperature, γ, usually have somewhat smaller effects. The dimensionless ambient temperature, γ, controls the thermal expansion of gas inside the channel.

These results of the non-radiative burning theory show reduced burning for two surfaces as compared to a single surface. We thus conclude that the so-called "chimney effect" associated with increased burning rates must be due to the entrapment of both flame and solid surface radiation or possible chemical kinetic effects.

Finally, the experimental results agree with the theoretical calculations. In the open regime, the opposing surface preserves the radiation heat; thus, the burning rate increases about 10–15 per cent more than single surface burning for methanol.

Acknowledgements—The authors are indebted to Professor Howard W. Emmons of Harvard University and Dr. Raymond Friedman of Factory Mutual Research Corporation for their continued encouragement in the course of this work.

REFERENCES

1. Y. B. Zeldovich, On the theory of combustion of initially unmixed gases, N.A.C.A. T.M. 1296 (1951).
2. D. B. Spalding, The combustion of liquid fuels, *4th Symposium (International) on Combustion*, p. 847. Williams & Wilkins, Baltimore (1953).
3. H. W. Emmons, The film combustion of liquid fuel, *Z. Angew. Math. Mech.* **36**, 60–71 (1956).
4. J. de Ris, Spread of a laminar diffusion flame, *12th Symposium (International) on Combustion*, The Combustion Institute, pp. 241–252 (1969).
5. F. J. Kodson, F. A. Williams and C. Buman, Combustion of vertical cellulosic cylinders in air, *12th Symposium (International) on Combustion*, The Combustion Institute, pp. 253–264 (1969).
6. J. S. Kim, J. de Ris and F. Wm. Kroesser, Laminar free-convective burning of fuel surfaces, *13th Symposium (International) on Combustion*, The Combustion Institute, pp. 949–961 (1971).
7. W. Elenbaas, Heat dissipation of parallel plates by free convection, *Physica* **9**(1), 1 28 (1942).
8. J. R. Bodoia and J. F. Osterle, The development of free convection between heated vertical plates, *J. Heat Transfer* **84**, 40–44 (1962).
9. P. M. Worsøe-Schmidt and G. Leppert, Heat transfer and friction for laminar flow of gas in a circular tube at high heating rate, *Int. J. Heat Mass Transfer* **8**, 1281–1301 (1965).
10. W. T. Lawrence and J. C. Chato, Heat-transfer effects on the developing laminar flow inside vertical tubes, *J. Heat Transfer* **88**, 214–222 (1966).
11. L. P. Davis and J. J. Perona, Development of free convection flow of a gas in a heated vertical open tube, *Int. J. Heat Mass Transfer* **14**, 889–903 (1971).
12. J. Quintiere and W. K. Mueller, An analysis of laminar free and forced convection between finite vertical parallel plates, *J. Heat Transfer* **95**, 53–59 (1973).
13. J. S. Kim, The burning of a vertical fuel surface, M.S. Thesis, Tufts University, Medford, Mass. (1969).
14. J. H. Perry, *Chemical Engineer's Handbook*, 4th ed., pp. 4 48. McGraw-Hill, New York (1963).
15. P. L. Howarth, On the solution of the laminar boundary layer equations, *Proc. R. Soc. Lond.* **164A**, 547–579 (1938); Concerning the effect of compressibility on laminar boundary layers and their separation, *Proc. R. Soc. Lond.* **194A**, 16–42 (1948).
16. W. F. Ames, *Numerical Methods for Partial Differential Equations*, p. 85. Barnes and Noble, New York (1969).

APPENDIX

An exact solution describing the overall physics of this problem would require the solution of elliptic partial differential equations including the second order diffusion terms of momentum, heat and species in the longitudinal direction. The mathematical solution of such elliptic equations is quite complex and would require at least an order-of-magnitude more computing time to solve, as compared to the present parabolic boundary layer equations, equations (2), (3) and (4) which regard the longitudinal diffusion terms to be an order of magnitude smaller than the other terms. In this appendix, the possible error of the boundary layer approximation will be examined using the boundary layer results to estimate the magnitude of the longitudinal gradients and comparing them to the transverse gradients so as to establish a criteria for the validity of this boundary layer solution.

The magnitude of the possible errors resulting from the neglect of the longitudinal diffusion terms can be represented by their ratio with the transverse diffusion terms, namely

$$\frac{\text{Longitudinal diffusion}}{\text{Transverse diffusion}} \sim \frac{\alpha|\Delta^2\Gamma/(\Delta x)^2|}{\alpha|\Delta^2\Gamma/(\Delta y)^2|} \sim \left(\frac{\Delta y}{\Delta x}\right)^2\Bigg|_{\Gamma=\text{const.}}$$

where Γ is any property which is transferred both by convection and conduction and α is the generalized molecular diffusivity of that particular property. Thus the possible error of the solution at a particular point can be expressed as a simple function of the slope of the equi-property lines at the point. The most convenient equi-property line is the flame where the specie concentrations and temperature are constant throughout. The above equation is now converted into its dimensionless form using the longitudinal dimensionless distance, X defined by equation (21) and the normalized transverse distance, Y.

$$\frac{\text{Longitudinal diffusion}}{\text{Transverse diffusion}}\Bigg|_{\text{flame}} \sim H^2\left(\frac{b}{l}\right)^2\left(\frac{\Delta Y}{\Delta X}\right)^2_{\text{flame}}$$

where $Y = y/b$.

The above equation shows that the error is inversely proportional to the square of the geometrical slope of the flame. The flame typically has an S-shape profile with local maxima of $\Delta Y/\Delta X$ at two points, one at the entrance and the other at the point where the flame intersects the center line. The point where the flame intersects the center line is obviously not important since, even though the transverse diffusion is zero, the flow is dominated by a strong longitudinal convection with relatively small vertical gradients in F or ψ. But at the entrance, the longitudinal gradients are dominant and the error for the boundary layer solution at this region could be large.

For the set of channels having a given value of H, the slope, $\Delta Y/\Delta X$, at the flame decreases sharply as the level, X, increases, thus reducing the error for larger values of X. Fixing both H and X, that means at a fixed fraction of the total height of channels having the same H, the only remaining factor which controls the error is the aspect ratio, l/b. Thus, increasing the aspect ratio, one can maintain the possible error at a given dimensionless elevation, X, to be less than any desired value.

Here a minimum acceptable aspect ratio, l/b, is calculated by first finding the fractional height, X/H, up to the point where 10 per cent of the total mass transfer at the surface has occurred and then adjusting l/b such that the longitudinal diffusion is 10 per cent (or 100 per cent) of the transverse

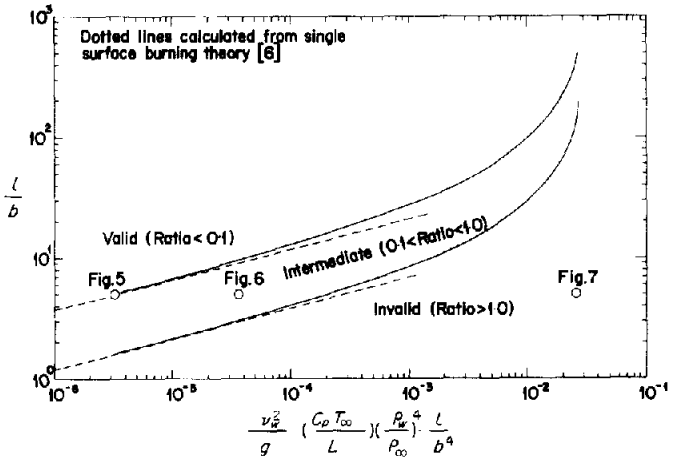

FIG. 9. Error criteria for burning methanol. *Ratio:* the maximum ratio of vertical diffusion to horizontal diffusion over the channel length for which 90 per cent of the total mass transfer occurs. Thus *Valid zone:* more than 90 per cent of total mass transfer takes place where vertical diffusion is less than 10 per cent of horizontal diffusion. *Intermediate zone:* more than 90 per cent of total mass transfer takes place where vertical diffusion is less than 100 per cent but more than 10 per cent of horizontal diffusion. *Invalid zone:* less than 90 per cent of total mass transfer takes place where vertical diffusion is more than 100 per cent of horizontal diffusion. The points indicate the errors for the specific flows shown in Figs. 5–7, respectively.

diffusion at the point. In this way one insures that 90 per cent of the total mass transfer occurs in a region for which the longitudinal diffusion is less than 10 per cent (or 100 per cent) of the transverse diffusion. Figure 9 shows these minimum aspect ratios against the dimensionless channel height, H, for the burning methanol.

The curves of 10 and 100 per cent ratios divide the entire zone into three parts. The lowest part is the zone where the longitudinal diffusion is larger than the transverse diffusion at the 10 per cent vaporization point; therefore, the boundary layer approximation fails to give a correct solution below this aspect ratio. However, in the uppermost zone, the longitudinal diffusion is always less than 10 per cent of the transverse diffusion at the point of 10 per cent vaporization; thus, the error on the total burning rate is much less than 10 per cent, perhaps closer to 1 per cent. In between, the longitudinal diffusion is between 10 and 100 per cent of transverse diffusion at the 10 per cent mass transfer point; thus, the solution is approximately correct. It has to be emphasized that the criteria are calculated at the point of 10 per cent vaporization; thus, at higher elevations the error is less than the prescribed one.

It is interesting to compare these results to the error of the single vertical surface burning theory [6]. In this theory, the flame distance from the fuel surface is proportional to a quarter power of the vertical distance. The identical error criteria can be expressed by lines of quarter power slope which are also shown in Fig. 9 by dotted lines. As the dimensionless channel height, H, decreases (left side of Fig. 9), the channel lies in the open regime and the errors of the present theory asymptotically approach that of the single surface burning theory.

COMBUSTION LAMINAIRE ENTRE DEUX SURFACES COMBUSTIBLES

Résumé—On a étudié théoriquement et expérimentalement des facteurs influençant la vitesse de combustion entre deux plaques combustibles verticales et en regard. On suppose: l'absence de rayonnement, des vitesses de réaction de la phase gazeuse infinies et un nombre de Lewis égal à l'unité.

La résolution numérique des équations a montré que le flux de combustion est contrôlé par le produit du nombre de Grashof, par le rapport de forme du canal (la demi-largeur du canal divisée par la longueur). Pour une grande largeur de canal, le flux de combustion est indépendant de cette distance et les résultats se ramènent à la solution pour une combustion sur surface unique.

Pour des canaux très étroits, le flux de combustion devient indépendant de la longueur du canal et il approche asymptotiquement une solution analytique obtenue pour des canaux infiniment longs.

Enfin, les résultats théoriques sont comparés aux résultats de l'expérience et il en résulte un accord favorable.

LAMINARE VERBRENNUNG ZWISCHEN ZWEI BRENNSTOFF-OBERFLÄCHEN

Zusammenfassung—Die Einflußfaktoren für die Verbrennung zwischen zwei vertikalen, parallelen Brennstoffoberflächen wurden theoretisch und experimentell untersucht. Angenommen wurde dabei: keine Strahlung, unendliche Reaktionsgeschwindigkeit in der Gasphase und eine Lewis-Zahl = 1.

Die Gleichungen werden numerisch gelöst; es wurde gefunden, daß die Verbrennung durch das Produkt aus Grashof-Zahl und Kanal-Anordnungsverhältnis (d.h. halbe Breite des Kanals geteilt durch seine Länge) bestimmt wird. Bei großem Oberflächenabstand ist die Verbrennung unabhängig von der Kanalweite und die Ergebnisse reduzieren sich auf unsere Lösungen für die Verbrennung an einer einzelnen Oberfläche. Für sehr lange, enge Kanäle wird die Verbrennung unabhängig von der Kanallänge und nähert sich asymptotisch der analytischen Lösung für unendlich lange Kanäle.

Die theoretischen Ergebnisse zeigen gute Übereinstimmung mit den experimentellen Daten.

ЛАМИНАРНОЕ ГОРЕНИЕ МЕЖДУ ДВУМЯ ТОПЛИВНЫМИ ПОВЕРХНОСТЯМИ

Аннотация — Теоретически и экспериментально исследовались факторы, влияющие на интенсивность горения между двумя вертикальными параллельными топливными поверхностями, расположенными друг против друга. Принималось, что число Льюиса равно единице, излучение отсутствует и скорость реакции в газовой фазе бесконечна.

Уравнения решались численно. Найдено, что интенсивность горения определяется произведением числа Грасгофа на отношение ширины канала к его длине (т. е. половина ширины канала, деленная на его длину). Для канала с большим поперечным сечением интенсивность горения не зависит от ширины канала, а результаты сводятся к полученному нами ранее решению для горения на одной поверхности. В случае очень длинных узких каналов интенсивность горения не зависит от длины канала и асимптотически приближается к аналитическому решению для бесконечно длинных каналов. И наконец, проведено сравнение теоретических результатов с экспериментальными, и получено хорошее соответствие.